# Optical kicked system exhibiting localization in the spatial frequency domain

**Amir Rosen, Baruch Fischer, and Alexander Bekker**

*Department of Electrical Engineering, Technion—Israel Institute of Technology, Haifa 32000, Israel*

**Shmuel Fishman**

*Department of Physics, Technion—Israel Institute of Technology, Haifa 32000, Israel*

Received February 1, 2000; revised manuscript received May 4, 2000

An optical kicked system with free-space light propagation along a sequence of equally spaced thin phase gratings is presented and investigated. We show, to our knowledge for the first time in optics, the occurrence of the localization effect in the spatial frequency domain, which suppresses the spreading of diffraction orders formed by the repeated modulation by the gratings of the propagating wave. Resonances and antiresonances of the optical system are described and are shown to be related to the Talbot effect. The system is similar in some aspects to the quantum kicked rotor, which is the standard system in the theoretical studies of the suppression of classical (corresponding to Newtonian mechanics) chaos by interference effects. Our experimental verification was done in a specific regime, where the grating spacing was near odd multiples of half the Talbot length. It is shown that this corresponds to the vicinity of antiresonance in the kicked system. The crucial alignment of the gratings in-phase positioning in the experiment was based on a diffraction elimination property at antiresonance. In the present study we obtain new theoretical and experimental results concerning the localization behavior in the vicinity of antiresonance. The behavior in this regime is related to that of electronic motion in incommensurate potentials, a subject that was extensively studied in condensed matter physics.  [S0740-3224(00)01208-X]

*OCIS codes:* 270.1670, 060.5530.

## 1. INTRODUCTION

The fields of classical optics and quantum mechanics describe wave phenomena. The small-wavelength limit of these theories is geometrical optics and classical Newtonian mechanics. In some situations there is a quantitative correspondence between wave optics and quantum mechanics.[1,2] Much was learned about one theory from the other one. The present study is based on extensive research performed on the quantum-mechanical localization found for the kicked rotor,[3,4] which was initiated by research on plasma physics and inspired by the exploration of electronic motion in disordered solids.[5,6] The ideas developed in the studies of the quantum kicked rotor are applied to classical optical systems, which are described by the same wave equation with a similar applied potential. It is in such a study that we achieve several goals. First, we apply and find new ideas in optics and also new possibilities for experiments that might be easier to perform in optics. This can also shed new light on the quantum-mechanical case. In the present study we give an experimental verification of localization in an optical system, which is an important addition to the sole demonstration, obtained only in recent years, of a quantum kicked rotor.[7,8] To our knowledge, this is the first experimental realization of an optical kicked system. In addition, motivated by our optical system, we find new features in a study of resonances and antiresonances, which are related to the Talbot effect[9] and are described here in detail. Below in this section we give a short introduction to both the concept of a quantum rotor and its role in the study of quantum chaos and localization.

The classical dynamics of chaotic systems were explored extensively during the past century, and the explorations intensified with the advent of computers.[10–14] The motion of such systems looks randomlike, although it is generated by simple deterministic equations. We confine ourselves to the exploration of Hamiltonian systems, where phase-space volume is conserved. Also, the quantal behavior of systems that are chaotic in the classical limit was studied extensively in recent years.[4,14–16] This field is sometimes called quantum chaos. For bound systems with time-independent Hamiltonian equations, the spectrum is discrete, and the motion is quasi periodic, and therefore it definitely cannot be considered chaotic. For systems with time-dependent Hamiltonian equations, the energy is not a good quantum number, and the phase space is in general not bounded. Consequently, there is no such general argument about the asymptotic nature of the quantum dynamics, which rules out its being chaotic. Classically, for these systems, diffusion in phase space is found. This diffusion is often suppressed by quantum interference effects[3,4,17–19] through a mechanism that is very similar to Anderson localization, namely, suppression of electronic diffusion in disordered solids at low temperatures.[5,6] The standard system for the exploration of the suppression of the classical diffusion by quantum interference is the kicked rotor. It can be visualized as a charged particle constrained to move on a frictionless

 

ring, in a uniform electric field directed in the plane of the ring, which is pulsed in equal time intervals. To study the quantal behavior various microscopic realizations were suggested.[20,21] So far, only one type of direct experimental demonstration of localization for the quantum kicked rotor, with laser-cooled Na and Cs atoms in a magneto-optic trap, has been reported.[7,8] Suppression of a similar nature was detected for driven atoms.[22]

Anderson localization is actually a wave phenomenon; therefore it can also be observed for classical electromagnetic waves. This phenomenon was indeed found in position space for truly random optical systems.[23–25] It was proposed as a tool for the study of the suppression of classical chaos by wave effects in the mode space of optical systems[26,27] and in the time domain of dispersive fibers.[28] Geometrical optics plays the role of classical mechanics, while wave optics plays the role of quantum mechanics. Moreover, in the paraxial approximation the Maxwell equations take the form of the Schrödinger equation, where the direction of propagation corresponds to the time in the Schrödinger equation.[1,2] In particular, kicked rotor realization was proposed to be done in dielectric optical fibers.[27] To our best knowledge, the experiments proposed in Refs. 26 and 27 have not yet been performed. In this paper we present what is to our knowledge the first experimental realization of an optical kicked system. We examine the localization properties in a specific regime near antiresonances of the system. Resonances and antiresonances in our optical system are shown to be related to the Talbot effect and were used by us to adjust critical parameters in the experimental system. A short report of the experimental study was given previously.[29]

We describe in Section 2 the optical kicked rotor system and in Section 3 the experimental setup. Then, in Section 4 we study theoretically the kicked rotor near antiresonance, which is relevant for the present experiment but is also of theoretical interest in its own right. A discussion and a comparison between theory and experiment is given in Section 5. In Appendix A we describe the Talbot effect and its relation to resonances and antiresonances, and in Appendix B we present the analytical solution of the linear kicked rotor, following Ref. 30.

## 2. OPTICAL KICKED ROTOR

In our optical kicked rotor system, schematically described in Fig. 1, a free-space-propagating light beam along the $z$ axis is successively kicked by identical thin sinusoidal phase gratings. The gratings are parallel, with an identical spacing $z_0$ between adjacent gratings,

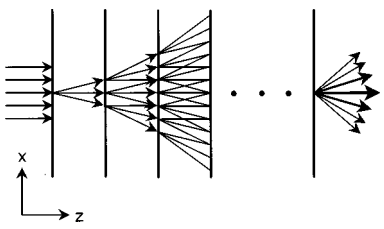


Fig. 1. Schematic description of the free-space kicked optical system with the array of phase gratings at equidistant locations. Some of the light paths are shown.

and have aligned phases. In the process the successive kicks produce high-order diffractions, which tend to increase the beam's spatial frequency band. Nevertheless, as we show below, localization in the spatial frequency domain, with a characteristic exponential confinement, occurs after several kicks. In the classical regime diffraction leads to nonlocalized diffusive behavior. This corresponds to the case in which the light intensities resulting from the gratings' diffraction are added up instead of the electric field amplitudes. In our experiment a regime of similar behavior is obtained when the grating phases are randomly positioned in the system, resulting in a destructive interference that behaves like the destruction of wave coherence.

The transverse ($x$-coordinate) dependence of the light electric field envelope $\psi$ is given, in the slowly varying amplitude (paraxial) approximation, by the following Schrödinger-like propagation equation[31]:

$$i\frac{\partial\psi}{\partial z} = -\frac{\lambda}{4\pi}\frac{\partial^2\psi}{\partial x^2} + \kappa\cos(k_g x)\sum_N \delta(z - Nz_0)\psi, \quad (1)$$

which includes the kick delta functions' potential, resulting from the phase sinusoidal gratings with a wave vector $k_g$ and an amplitude $\kappa$, while $\lambda$ is the light wavelength. Here the coordinate $z$ along the direction of propagation plays the role of time for the kicked rotor. The intensity is proportional to $|\psi|^2$.

In analogy with the case of a quantum kicked rotor, the Hamiltonian-like operator is

$$\mathcal{H} = \gamma\hat{n}^2 + V(x, z), \quad (2)$$

where $\hat{n} = -i\{\partial/[\partial(k_g x)]\}$ is the normalized transverse spatial frequency operator in the kinetic-energy-like term, $V(x, z) = \kappa\cos(k_g x)\Sigma_N\delta(z - Nz_0)$ is the propagation-dependent potential energy term, $\gamma = \pi\lambda z_0/\lambda_g^2$, and $\lambda_g = 2\pi/k_g$ is the grating period.

Unlike the quantum kicked rotor and the fiber realizations proposed in Ref. 27, our optical system lacks inherent discrete energy levels in the light transverse spatial frequency domain. It shares this property with driven laser-cooled atoms.[7,8] However, when the input light is a plane wave or a broad Gaussian beam, the sinusoidal grating kicks confine the dynamics to the discrete frequency modes of the gratings' diffraction orders $n$ (corresponding to the angular momentum of the kicked rotor), which are coupled among themselves. If the initial mode is $n = 0$, as is the case in our experiment, only modes with integer $n$ are involved in the evolution. In this process the repeated kicks tend to broaden the number of the diffraction orders. The propagation between the successive kicks adds extra phases, $\exp(-i\gamma n^2)$, which are quadratically dependent on the diffraction order $n$. For large $n$, this factor behaves like a random number. The resulting one-period evolution operator is

$$\hat{U}_{\mathrm{KR}} = (\exp - i\gamma\hat{n}^2)\exp[-i\kappa\cos(k_g x)]. \quad (3)$$

As a result of the effective randomness of the factors $\exp(-i\gamma n^2)$, it turns out that the overall contribution is weakened, resulting in exponential localization that is similar to Anderson localization in disordered solids.[3–6] Consequently, low $n$ are mostly composed of former low-

order harmonics, which are added constructively. It is crucial that the propagator $\hat{U}$ is identical for all kicks. Although $\exp(-i\gamma n^2)$ behave like random numbers, these are identical for all intervals of free motion. The spread in the space of the spatial frequency modes (diffraction orders), $\sigma \equiv \sqrt{\langle (n - \langle n \rangle)^2 \rangle}$, was calculated by numerical integration of Eq. (1), which can easily be done by propagation of Eq. (3), step by step, with a fast-Fourier-transform technique. The results for experimentally realistic parameters are presented in Fig. 2. Geometrical optics, where intensities rather than amplitudes are evolved, predicts diffusion in spatial frequency space. This spread is found to be similar to the one obtained for phase-disordered gratings, where we add for each grating $N$ a random phase, $\varphi_N$, such that $\gamma n^2$ is replaced by $\gamma n^2 + \varphi_N n$. A similar diffusive behavior is obtained for random $\gamma$. This corresponds to an experiment in which the spacing between the adjacent gratings is not accurately adjusted. In the calculations of Fig. 2, as well as in all the other numerical calculations, the initial state is $n = 0$, corresponding to the experiment, resulting in $\langle n \rangle = 0$.

For typical aligned gratings, where $\gamma/\pi$ is an arbitrary irrational number, one finds in this case that the onset of localization takes place after 25 gratings. Because of absorption this localization regime is experimentally inaccessible. Near antiresonance, where $\gamma \approx (2M + 1)\pi$ with integer $M$, the onset of localization is immediate. This regime is also experimentally advantageous, since the phases of the gratings can be simply aligned at antiresonance. It is also of special theoretical interest because in the vicinity of antiresonance the kicked rotor behaves like the two-sided kicked rotor, which has been the subject of theoretical investigations.[32] In the vicinity of the antiresonance the localization behavior can be approximated by the exactly solvable linear kicked rotor,[30] with a linear dependence on $n$ of the phases in the free-space-propagation term $\exp(-i\tau n)$. This model was studied previously and was mapped onto a model for electronic motion in potentials with incommensurate periods.[30] Such models were studied extensively in condensed matter[33–38] and in mathematical physics.[39–41] The linear kicked rotor that locally approximates the kicked rotor near antiresonance was found to exhibit localization that is stronger than the exponential.[30]

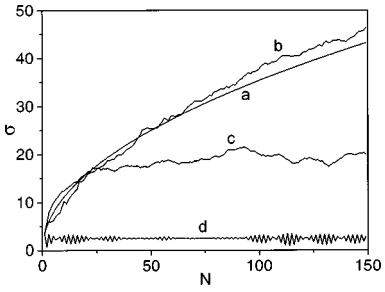


Fig. 2. Numerical simulation of the evolution of the spatial frequency width $\sigma$ as a function of the number of kicks $N$, for a classical system (without interference) that exhibits diffusive behavior (curve a) and for phase-disordered gratings (where we added for each grating $N$ a random phase, $\varphi_N$, such that $\gamma n^2$ is replaced by $\gamma n^2 + \varphi_N n$; curve b). A similar diffusive behavior was obtained for random $\gamma$. Confinement behavior is obtained for ordered gratings, far from resonance or antiresonance (with $\gamma = 0.74\pi$; curve c) and near antiresonance (with $\gamma = 2.97\pi$, or $\delta = -0.03$; curve d). For all graphs, $\kappa = 5.94$, which matches the experiment, and the starting state is $n = 0$, resulting in $\langle n \rangle = 0$.

## 3. EXPERIMENT

The experimental setup followed the schematic description given in Fig. 1. It can immediately be realized that the grating positioning, and especially their phase alignment, is most crucial. For this reason, we developed a special technique that gave us access to a specific regime of localization. This was the vicinity of antiresonances of our optical system, which are related to half-Talbot distances.

The Talbot effect,[9] described and explained in Appendix A, is the occurrence of optical self-imaging of periodic images along propagation in free space at multiple distances of the Talbot length, $z_T = 2\lambda_g{}^2/\lambda$ ($\gamma = 2\pi$). Thus, when the gratings' spacing in our system equals the Talbot length, it is equivalent to the case in which the free-space propagation shrinks to zero. Then all the gratings are coherently added in phase, without any dephasing factor of the space between the adjacent ones, and the diffraction orders steadily increase with the number of gratings. This corresponds to a resonance like state resembling the resonances in the quantum rotor case. By contrast, the system with grating locations at half-Talbot distances (odd multiples of $z_T/2$) corresponds to antiresonance, where any two successive (aligned) gratings cancel each other. Here the propagation after the first grating produces at the second grating the same periodic image, but it is shifted by $\pi$, which is then canceled by the second grating. This effect of diffraction cancellation enabled us to accurately adjust the grating locations and align their phases. We performed the alignment in a reverse way, from the final (output) grating toward the first, by checking that each added grating canceled the diffractions that were due to the former grating. The accuracy demand in the other alignment parameters was less critical. Small deviations in the exact distances between the adjacent gratings, which affect the phases through $\gamma n^2$, had a tolerance of the order of 0.1 mm for $n \sim 5$.

After the alignment was done we changed the laser wavelength, $\lambda$, to move the system away from the trivial antiresonance state. In the experiment we aligned the system with the argon-ion laser line $\lambda = 501\,\mathrm{nm}$, with a spacing of $z_0 = (3/2)z_T = 3.832\,\mathrm{cm}$ ($\gamma = 3\pi$) for $\lambda_g = 80\,\mu\mathrm{m}$, and made the measurement at $\lambda = 496\,\mathrm{nm}$, which gave $\gamma = 2.97\pi$. The strength of the kick by the grating was $\kappa = 5.94$. It was important in our experiment to stay near antiresonance because of the limited number of gratings that we could use. The first reason for this is absorption. In addition, the gratings' size becomes a more limiting factor as the beam propagates and spreads in real space in the transverse direction of the beam, owing to the diffraction. The spot size of the spatially filtered input beam to the system was quite large, ~4 cm, allowing significant interference of the diffracted

beam as it propagated along the gratings. Nevertheless, smaller spot sizes were examined, as described below.

The phase gratings in the experiment were prepared by a holographic method, with 8E75 Agfa-Gevaert plates. We chemically bleached the plates to obtain the conversion from amplitude to phase holograms. The size of each grating slide was 6.5 cm × 3 cm. The emulsion, or the gratings' thickness, was ~5 $\mu$m. In our system this can be regarded as a delta-function kick.[27]

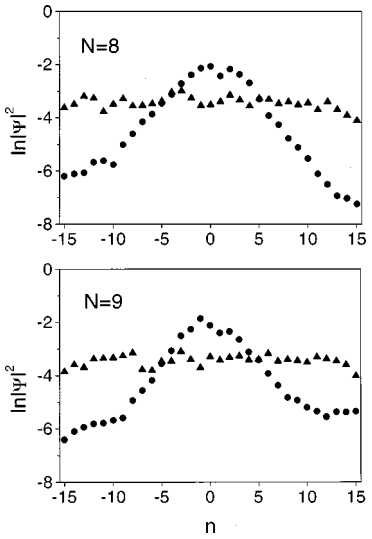


Fig. 3. Experimental confined spatial frequency spectrum intensity after the eighth and ninth gratings for the ordered (filled points) and disordered (filled triangles) gratings. The initial direction is $n = 0$, within experimental accuracy.

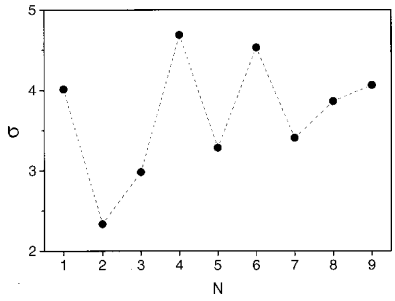


Fig. 4. Experimental spatial frequency intensity width $\sigma$ after each of the nine kicks (the symbols are the same as in Fig. 3).

The spatial frequency analysis of the light was done at the far field of the output beam. The measurement was done by a detector array, on which the far field was imaged by a large-aperture lens.

The central experimental result is presented in Fig. 3. It shows the confinement of the light spatial frequency after the eighth and ninth gratings for the ordered grating system, as compared with the spread spectrum without localization for a disordered system, where the gratings phases were not aligned. The spatial frequency intensity width after each of the nine kicks is shown in Fig. 4. Further details, with the analysis and a comparison with the theory, are given below.

## 4. THEORETICAL ANALYSIS OF THE KICKED ROTOR NEAR ANTIRESONANCE

In this section the kicked rotor defined by Eq. (1) will be studied near the antiresonance, where $\gamma \approx (2M + 1)\pi$, with integer $M$. We first present the main features of the dynamics in this regime, which are obtained by numerical calculations. We then obtain the main properties with the help of the local approximation of the kicked rotor by the linear kicked rotor, which is applicable near antiresonance.

The long-term localized spectrum (light intensity as a function of the diffraction order $n$), calculated numerically near antiresonance, is given in Figs. 5 and 6. Here we carried out a numerical calculation propagating a broad plane wave in the system, kick after kick, with the application of the propagator in Eq. (3). It has a fir-tree shape with a slightly faster than exponential decay, as is given by the analysis for localization in this regime, which corresponds to the linear kicked rotor[30] (see discussion given immediately below). The added plateaus, each of which is shown in Figs. 5(c) and 6(c), have a more moderate exponential decay.

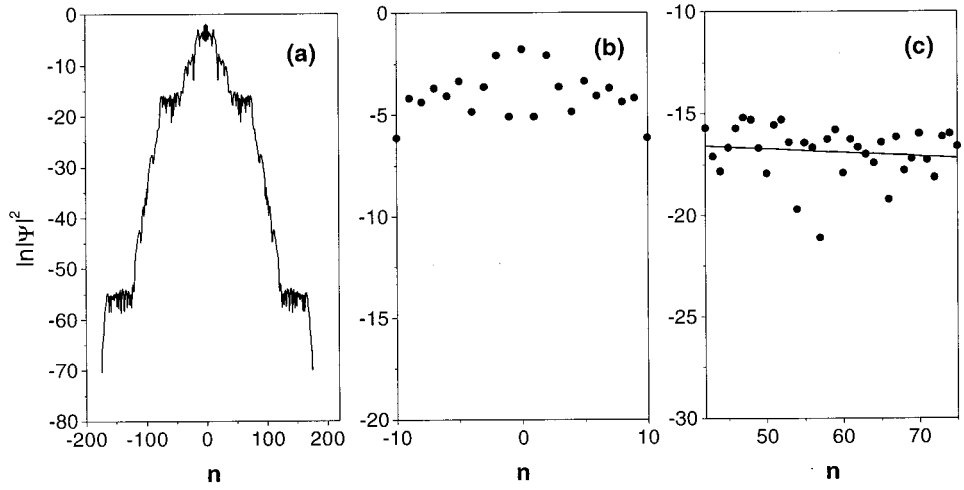


Fig. 5. (a) Typical numerically calculated confined spatial frequency spectrum $|\psi|^2$, with a fir-tree shape after $N = 200$ kicks, starting from a wave with $n = 0$. We used $\kappa = 15$ and $\delta = 0.011$. Zooms of tree head and one of the plateaus are given in (b) and (c), respectively.

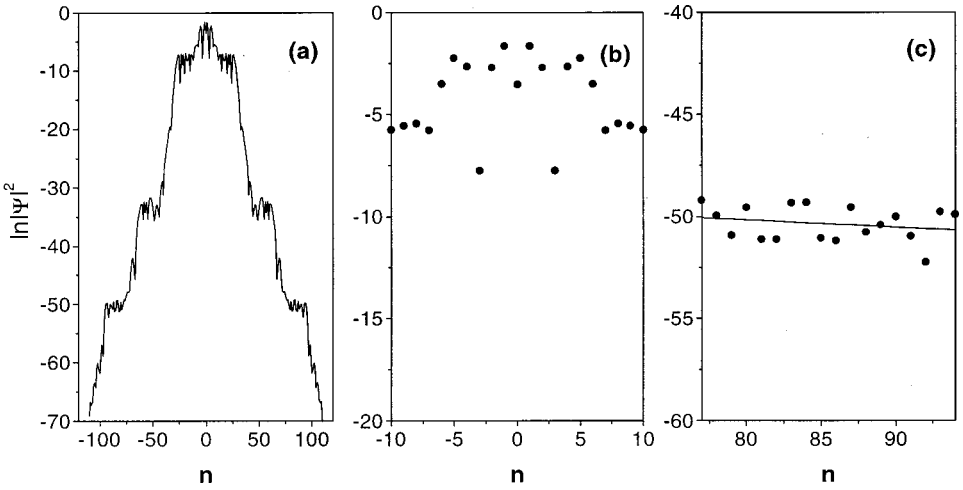


Fig. 6. Same as Fig. 5, but for $\kappa = 5.94$ and $\delta = -3 \times (5/501) \approx -0.03$, corresponding to the experimental parameters.

The results for the spreading near the antiresonance can be understood from the correspondence with the linear kicked rotor. Near antiresonance, $\gamma = (2M + 1)\pi + \delta\pi$, where $M$ is an integer ($M = 1$ in the present experiment) and $\delta \ll 1$. For $n \ll n_0$, the local approximation $(1/2)\delta(n + n_0)^2 \approx \delta n_0 n + C$ can be made, when $(1/2)\delta n^2 \ll 1$, and where the constant $C = (1/2)\delta {n_0}^2$. Using the fact that $\exp[-i\pi(2M + 1)n^2] = \exp(-i\pi n)$, one can approximately write the free-propagation part of $\hat{U}_{\mathrm{KR}}$ as $\exp[-i\gamma(n_0 + n)^2] \approx \exp\{-i[(\pi + \tau)n + \text{const.}]\}$, where $\tau = 2\pi\delta n_0$. Because of the smallness of $\delta$, the parameter $\tau$ varies slowly with the center of the expansion, $n_0$, and will be assumed constant. The resulting local model can be defined by the one-step evolution operator

$$\hat{U}_{\mathrm{LR}} = \exp[-i\kappa\cos(k_g x)]\exp[-i(\tau + \pi)\hat{n}]. \quad (4)$$

The quasi-energy states of this evolution operator, which are obtained in Appendix B according to Ref. 30, are

$$\psi_\nu(n) = \exp[i(\tau/2)(n - \nu)] \times (-i)^{|n-\nu|} J_{|n-\nu|}\left\{\frac{\kappa}{2\sin[(\tau + \pi)/2]}\right\}, \quad (5)$$

where $\nu$ is the center of localization and $J_n$ are Bessel functions. If the Bessel functions decay rapidly, as is the case when the index is much larger than the argument in magnitude, the linear approximation holds, since $\tau$ can be considered constant in a range in which the Bessel function varies considerably. Therefore the approximation is expected to fail where this argument is large, i.e., at the points where $\sin[(\tau + \pi)/2] = 0$ or $n_0^{(l)} = (2l - 1)/2\delta$, where $l$ is an integer. In the regions that are far from $n_0^{(l)}$ the eigenfunctions fall off locally as Bessel functions, resulting in the rapid falloff of intensity in Figs. 5 and 6. Below we analyze individual eigenfunctions and verify in detail this form of decay. We find that the plateaus in Fig. 5 are starting from $n_0^{(l)} = 50, 150, 250...$ [$n_0^{(l)}$ is the point on the plateau that is the closest to the origin], corresponding to $l = 1, 2, 3...$ for $\delta = 0.01 \approx 1/100$. There is also a plateau around $n = 0$, where $n \ll n_0$ is not satisfied. In Fig. 6 we used $\delta = -3 \times (5/501) \approx -0.03$, and the plateaus start from $n_0^{(l)} = 17, 50, 83...$, corresponding to $l = 1, 2, 3...$. The width of the plateaus, $\Delta n_0$, can be estimated, from the requirement for the linear approximation, to hold for some distances (somewhat larger than $\Delta n_0$) from $n_0^{(l)}$. In the vicinity of $n_0^{(l)}$ the argument of the Bessel functions (5) is approximately

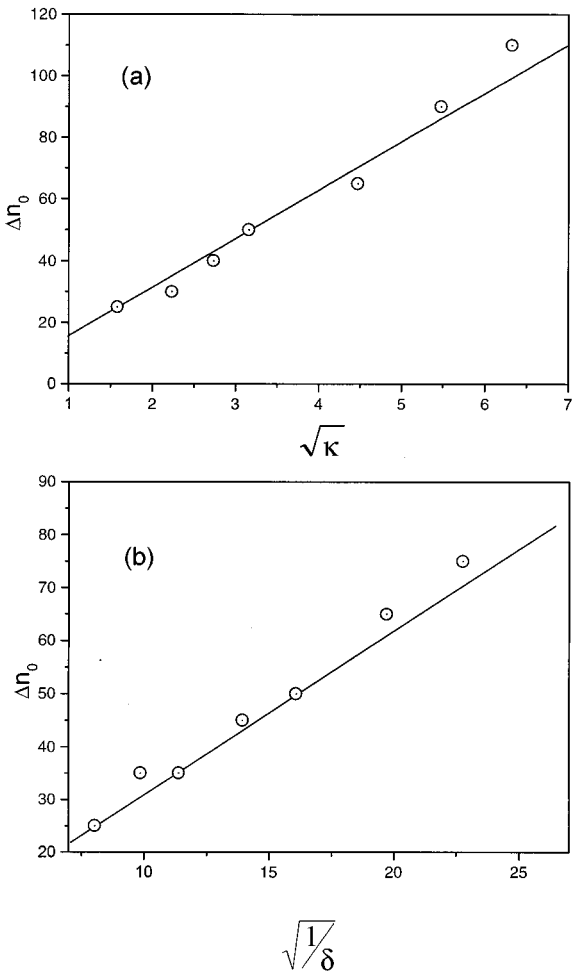


Fig. 7. Widths of the plateaus $\Delta n_0$ for various values of $\kappa$ and $\delta$, determined by visual inspection of figures like Figs. 5 and 6 (circles), as compared with relation (8), with $a = \sqrt{3/\pi}$ (solid lines), for (a) $\delta = (\sqrt{5} - 1)/320$ and variable $\kappa$ and for (b) $\kappa = 10$ and variable $\delta$.

$$d_A \approx \frac{\kappa}{2\pi\delta d_n}, \tag{6}$$

where $d_n = |n_0^{(l)} - n_0|$, as can be seen from the definition of $\tau$. For a site $n$ to be only weakly coupled to the region around $n_0^{(l)}$, where the linearized approximation fails, it is necessary that $|n_0^{(l)} - n|$ be larger than the argument of the Bessel function there. Therefore such a site should be outside a region of width $\Delta n_0$ around $n_0^{(l)}$, which satisfies

$$\Delta n_0 \approx \frac{\kappa}{2\pi\delta\Delta n_0} \tag{7}$$

or

$$\Delta n_0 \approx a\sqrt{\kappa/\delta}, \tag{8}$$

where $a$ is some numerical constant, of order unity, that cannot be found from this crude estimate. This relation was tested for various values of the parameters, and the results are presented in Fig. 7. The prefactor was found to be $a = \sqrt{3/\pi}$. Within the plateaus exponential decay was found. The values of the localization length found from Figs. 5(c) and 6(c) are $\xi = 38$ and $\xi = 60$, respectively.

What is the form of the eigenfunctions of the model (1) predicted by the linear approximation (4)? For small $\delta$, the linear approximation holds for most $n$, since the distance between the regions where it fails grows as $1/\delta$, while their width is $\Delta n_0 \sim \sqrt{1/\delta}$. In the regions where the linear approximation holds, the eigenfunctions of model (1) are superpositions of few eigenfunctions of model (4), centered in regions where the approximation fails [the values of $\nu$ in Eq. (5) are in that region]. The reason for this form is that the rate of decay is determined by the local properties of the equation, while the position of the center and the value of the quasi energy are determined by the normalization condition. To test the local approximation by the linear kicked rotor the eigenfunctions of the model (1) are compared locally with the eigenfunctions (5) of the linearized model (4). The results are presented in Fig. 8. The local eigenstates of the model depend on $\nu$ and on the parameter $\tau$, which depends on the position $n_0$. The eigenstates (5) depend on $\tau$ through $s = 2\sin[(\tau + \pi)/2]$, which for most $n_0$ values is weakly dependent on $\tau$. In the vicinity of $n_0^{(l)}$, $|s| < 1$, while far from these points $|s| \approx 1$. We do not know how to determine analytically the values of $\nu$ and $\tau$ for states that dominate a specific eigenstate of Eq. (1). In the numerical simulations values of $\nu$ and $\tau$ were chosen to demonstrate the validity of the local approximation for some values of $\nu$ and $\tau$, which was found to work very well. [A similar approximation was found for many eigenstates of Eq. (1).] An analytical method to determine these values has yet to be developed.

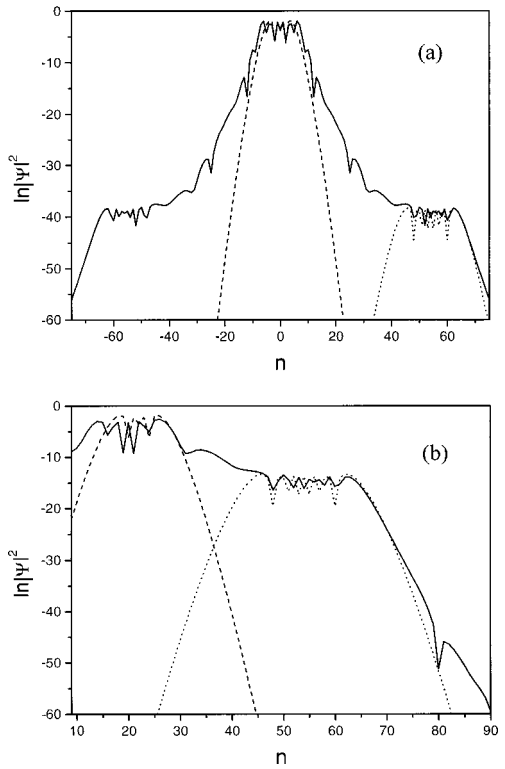


Fig. 8. Eigenstates of model (1) for $\kappa = 10$ and $\delta = 51/4096$ (solid curves): (a) eigenstate of Eq. (1), centered near the origin, and eigenstates (5) of Eq. (4), with $\nu = 0$ and $s = 1$ (dashed curve) and $\nu = 54$ and $s = 1/2$ (dotted curve); (b) eigenstate of Eq. (1), centered near $n = 20$, and eigenstates (5) of Eq. (4), with $\nu = 22$ and $s = 1$ (dashed curve) and $\nu = 54$ and $s = 1/2$ (dotted curve).

The kicked rotor model near antiresonance is simply related to the two-sided kicked rotor model near resonance. The evolution operator of the two-sided kicked rotor is

$$\hat{U}_{\mathrm{TS}} = \exp(-i\gamma_2\hat{n}^2)\exp[-i\kappa\cos(k_g x)] \times \exp(-i\gamma_2\hat{n}^2)\exp[+i\kappa\cos(k_g x)]. \tag{9}$$

The free-motion part of $\hat{U}_{\mathrm{KR}}$ near antiresonance can be written in the form

$$\exp(-i\gamma\hat{n}^2) = \exp(-i\pi\hat{n})\exp(-i\gamma_2\hat{n}^2), \tag{10}$$

where $\gamma = \pi(2M + 1) + \gamma_2$ and $M$ is an integer. Using

$$\exp(-i\pi\hat{n})\exp[-i\kappa\cos(k_g x)] = \exp[-i\kappa\cos(k_g x - \pi)]\exp(-i\pi\hat{n}) \tag{11}$$

and $\exp(-i2\pi\hat{n}) = I$, one finds that

$$\hat{U}_{\mathrm{KR}}^2 = \exp(-i\pi\hat{n})\hat{U}_{\mathrm{TS}}\exp(-i\pi\hat{n}), \tag{12}$$

which acts like $\hat{U}_{\mathrm{TS}}$.

## 5. DISCUSSION AND SUMMARY

A comparison of the theoretical and the experimental results is shown in both Figs. 9 and 10. Figure 9 gives the spatial spectrum intensities after eight and nine gratings, and Fig. 10 gives the spatial frequency widths $\sigma$. We showed, in Fig. 3, the experimental data for the disordered-gratings case, in which the localization was destroyed and a flat spread spectrum was obtained, as compared with the ordered-gratings case that exhibits confinement. The comparison between the spatial frequency width found in the experiment after each of the nine kicks and the theoretical predictions given in Fig. 10

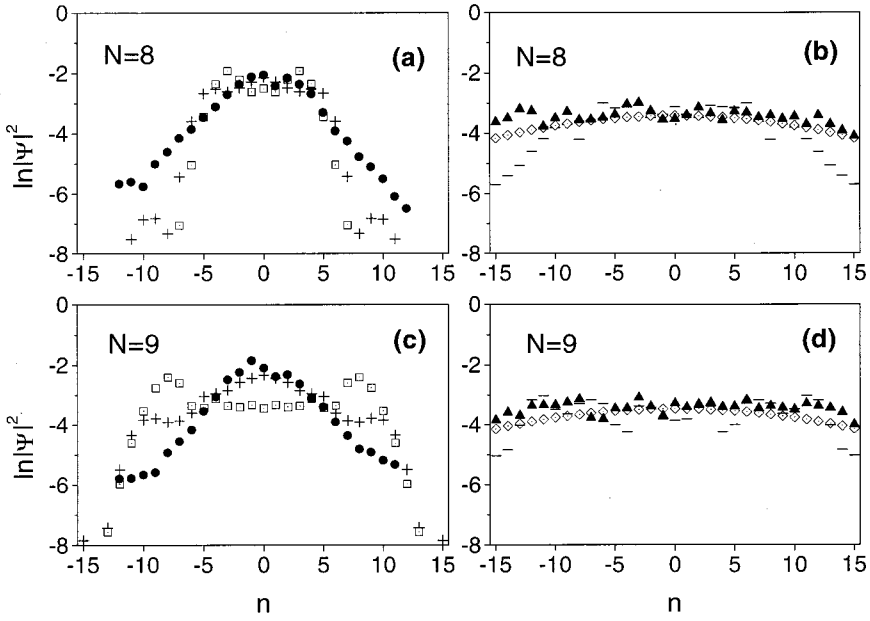


Fig. 9. Experimental spatial frequency spectrum intensity after the eighth [(a), (b)] and ninth [(c), (d)] gratings for ordered [filled circles in (a) and (c)] and phase-disordered [filled triangles in (b) and (d)], gratings, as compared with the theoretical results from Eq. (1), near antiresonance, where $\delta = -0.03$, showing localization [plus sign in (a) and (c)] or a spread spectrum away from antiresonance [minus sign in (b) and (d)], where $\gamma = \sqrt{5} - 1$, and when intensities, rather than field amplitudes, are used [diamonds in (b) and (d)], which gives results similar to the case in which the phase of the gratings is random. The results of the linear model (4), for $\tau = -0.18\pi$ ($\delta = -0.03$, $n_0 = 3$; squares), are presented as well.

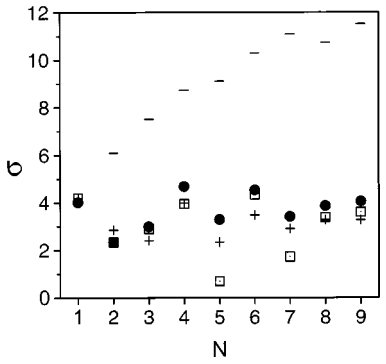


Fig. 10. Experimental spatial frequency intensity width $\sigma$ after each of the nine gratings (filled circles), as compared with the theoretical results of Eq. (1) near antiresonance (plus signs), with $\gamma = 2.97\pi$, and away from antiresonance (minus signs), where $\gamma = \sqrt{5} - 1$. Also shown is the result (squares) in the linear model with $\delta = -0.03$, $n_0 = 3$, which give $s = 1.92$.

shows a good agreement, even in the oscillating behavior, which is characteristic of the vicinity of antiresonances. The experimental confinement width was $\sigma \approx 3-4$. Exactly at antiresonance, where each even grating cancels the spreading that is due to its former odd grating, the oscillation of the width as a function of the grating number has a period of 2 (with values $\sigma_a$, 0, $\sigma_a$, 0, $\sigma_a$,0...), presenting a trivial confinement. Off antiresonance, but still in its vicinity, there is a more complex variation of $\sigma$, as can be seen in Figs. 10 and 4, as well as in the graph shown in Fig. 2(d). In the experiment we also checked the possible influence of the finite sizes of the input light and the gratings. We found no significant difference when we changed the spot size of the input beam from ≈4 to ≈1.5 cm. However, much smaller spot sizes can affect and change the diffraction and the strength of the localization effect.

Thus the Schrödinger equation (1) faithfully models the experiment. The linear approximation works well in the antiresonance regime, and the behavior there is very different from the one for a typical value of $\gamma$. The linear approximation clearly predicts the qualitative behavior and the correct order of magnitude, but not the detailed behavior for each grating.

In conclusion, we have presented what is to our knowledge the first experimental realization of an optical kicked system with localization. In this system, free-space propagation of light is periodically kicked by thin sinusoidal phase gratings. Our present study was mainly concentrated on the near-antiresonance regimes, where new theoretical properties and experimental results were obtained.

## APPENDIX A: TALBOT EFFECT, RESONANCES, AND ANTIRESONANCES IN THE OPTICAL KICKED SYSTEM

Here we present a more detailed description of the Talbot effect, relate it to resonances and antiresonances in the optical kicked system, and show the way that we used it to align the optical system.

As we described above, a periodic image reproduces itself, as it propagates in free space, at distances that are multiples of the so-called Talbot length $z_T$.[9] The reason for this can be seen very easily when the periodic function $\psi(x, z = 0) = \psi(x + m\lambda_g, z = 0)$ ($m$ is an integer), with periodicity $\lambda_g = 2\pi/k_g$, is expressed as a Fourier series:

$$\psi(x, z = 0) = \sum_n a_n \exp(ink_g x). \tag{A1}$$

Then, as we showed above, the propagation in free space, in the paraxial regime, adds to each component in the series the quadratically $n$-dependent phase factor $\exp(-i\gamma n^2)$, where $\gamma = \pi\lambda z/{\lambda_g}^2$, giving

$$\psi(x, z) = \sum_n a_n \exp(ink_g x - i\gamma n^2). \tag{A2}$$

When $\gamma = 2\pi N$ ($N$ is an integer), as occurs for $z = Nz_T = N2{\lambda_g}^2/\lambda$, we have

$$\psi(x, z = Nz_T) = \psi(x, z = 0), \tag{A3}$$

an exact reproduction of the image. At half-Talbot distances (odd multiples of $z_T/2$), where $\gamma = (2N + 1)\pi$, we have

$$\psi\left(x, z = (2N + 1)\frac{z_T}{2}\right) = \psi\left(x + \frac{\lambda_g}{2}, z = 0\right), \tag{A4}$$

or the periodic image is shifted by half a period.

In our optical system the kicks with the sinusoidal phase gratings modulate the light by the periodic function $\exp[i\kappa\cos(k_g x)]$, which is composed of, and produces, the various diffraction orders [with a weight $a_n = i^n J_n(\kappa)$, according to the corresponding components of the Fourier series in Eq. (A1)]. Then, in the case of a spacing of $z_T$ between the adjacent gratings, the light that reaches each grating perfectly matches the grating. Then all the gratings are coherently added in phase, without any scrambling factor of the space between them. The situation here is equivalent to the case in which the free-space propagation shrinks to zero. This corresponds to a resonance state, and the diffraction orders steadily increase with the number of gratings.

By contrast, the system with grating locations at half-Talbot distances (odd multiples of $z_T/2$) corresponds to antiresonance, where the effect of any two successive (aligned) phase gratings cancel each other. Here the propagation of the modulated field amplitude $\exp[i\kappa\cos(k_g x)]$, from the first grating to the second grating, produces a $\pi$-shifted sinusoidal image, $\exp[i\kappa\cos(k_g x + \pi)]$, which is then multiplied and canceled by the phase modulation of the second grating, $\exp[i\kappa\cos(k_g x)]$, giving 1. This situation continues to occur for the rest of the gratings. The effect of cancellation at antiresonance enabled us to adjust the gratings, as described above.

The resonances and antiresonances of our optical system resemble those of the ordinary quantum kicked rotor. At resonance the coherent successive grating kicks produce a steady spreading and increase of the width in the spatial frequency domain (or in the diffraction orders' numbers), and consequently the energy increases in the quantum kicked rotor case. However, exactly at antiresonance, the cancellation of two successive kicks eliminates the spreading.

## APPENDIX B: SOLUTION OF THE LINEAR KICKED ROTOR PROBLEM

In this appendix we derive the eigenstates of the linear rotor, following Ref. 30. In the linear case the free-space propagation has a linear phase dependence on $n$, as compared with the quadratic dependence in the regular case. This does not describe the real physical behavior of the rotor or light propagation. Nevertheless, as we showed in the text, the linear rotor locally approximates the kicked system near antiresonance.

The linear system is defined by the equation

$$i\frac{\partial\psi}{\partial t} = \tau\hat{n} + \kappa\cos y\sum_N \delta(t - N)\psi, \tag{B1}$$

where $\hat{n} = -i[\partial/(\partial y)]$. Here we use the dimensionless variables, $t$ and $y$, which follow the quantum kicked rotor notation or correspond to the optical kicked system, by means of

$$t = z/z_0, \qquad y = k_g x. \tag{B2}$$

The one-step evolution operator is

$$\hat{U} = \exp(-i\kappa\cos y)\exp(-i\tau\hat{n}). \tag{B3}$$

The quasi-energy states are

$$\psi_\nu(y, t) = \exp(-i\omega_\nu t)\phi_\nu(y, t), \tag{B4}$$

where $\omega_\nu$ is the quasi energy and $\phi_\nu(y, t)$ is $2\pi$ periodic in $t$ and $y$. These are the eigenstates of $\hat{U}$, satisfying

$$\hat{U}\psi_\nu = \exp(-i\omega_\nu)\psi_\nu. \tag{B5}$$

Taking $\phi_\nu(y, t)$ just after each kick, one can suppress its time dependence. Because of unitarity, it takes the form

$$\phi_\nu(y) = 1/\sqrt{2\pi}\exp[i\varphi_\nu(y)], \tag{B6}$$

with

$$\varphi_\nu(y) = \nu y + \sum_l {C_l}^\nu \exp(ily). \tag{B7}$$

Substitution of the quasi-energy states of the form given in Eqs. (B6) and (B7) into Eq. (B5) yields

$$-\omega_\nu + \varphi_\nu(y) = -\kappa\cos y + \varphi_\nu(y - \tau), \tag{B8}$$

leading to

$$\omega_\nu = \nu\tau \bmod 2\pi, \tag{B9}$$

$${C_{\pm 1}}^\nu = \mp\frac{\kappa}{4i}\frac{\exp(\pm i\tau/2)}{\sin(\tau/2)}, \tag{B10}$$

while all the other ${C_l}^\nu$ values vanish. Therefore

$$\varphi_\nu(y) = \nu y - \frac{\kappa}{2}\frac{\sin(y + \tau/2)}{\sin(\tau/2)}. \tag{B11}$$

The eigenstates $\phi_\nu$ can be expanded in plane waves $1/\sqrt{2\pi}\exp(-iny)$. Since the kicking is $2\pi$ periodic in $y$, only components with integer $(n - \nu)$ are involved in the expansion. This expansion takes the form

$$\phi_\nu(y) = \exp(i\nu y)\sum_m i^m J_m\left[\frac{-\kappa}{2\sin(\tau/2)}\right] \times \exp\{-im[(\pi-\tau)/2-y]\} \quad \text{(B12)}$$

and, in the momentum representation,

$$\phi_\nu(n) = J_{n-\nu}\left[\frac{\kappa}{2\sin(\tau/2)}\right](-1)^{n-\nu}\exp[i(n-\nu)\tau/2]. \quad \text{(B13)}$$

Replacing $\tau$ with $\tau + \pi$, one obtains Eq. (5).

In this derivation it was implicitly assumed that $\tau/\pi$ is irrational. For $\tau = 2\pi(p/q)$ (where $p$ and $q$ are integers), there are $q$ infinitely degenerate quasi energies.[30] Note that, for $\tau = 2\pi l$ (with integer $l$), the solution (B13) diverges.

## ACKNOWLEDGMENTS

This work was partially supported by the Division for Research Funds of the Israel Ministry of Science, by the U.S.–Israel Binational Science Foundation, by the Minerva Center for Nonlinear Physics of Complex Systems, and by the Fund for Promotion of Research at the Technion.

B. Fischer can be reached by e-mail: fischer@ee.technion.ac.il.

## REFERENCES AND NOTES

1. A. W. Snyder and S. D. Love, *Optical Waveguide Theory* (Chapman & Hall, London, 1983).
2. D. Marcuse, *Theory of Dielectric Optical Waveguides* (Academic, New York, 1974).
3. S. Fishman, D. R. Grempel, and R. E. Prange, "Chaos, quantum recurrences, and Anderson localization," Phys. Rev. Lett. **49**, 509–512 (1982); D. R. Grempel, R. E. Prange, and S. Fishman, "Quantum dynamics of a nonintegrable system," Phys. Rev. A **29**, 1639–1647 (1984).
4. F. Haake, *Quantum Signatures of Chaos* (Springer, New York, 1991).
5. P. W. Anderson, "Absence of diffusion in certain random lattices," Phys. Rev. **109**, 1492–1505 (1958).
6. For reviews, see D. J. Thouless, "Critical phenomena, random systems, gauge theories," in *Proceedings of the Les-Houches Summer School*, K. Osterwalder and R. Stora, eds. (North-Holland, Amsterdam, 1986), p. 681; I. M. Lifshits, S. A. Gredeskul, and L. A. Pastur, *Introduction to the Theory of Disordered Systems* (Wiley, New York, 1988).
7. F. L. Moore, J. C. Robinson, C. F. Barucha, B. Sundaram, and M. G. Raizen, "Atom optics realization of the quantum $\delta$-kicked rotor," Phys. Rev. Lett. **75**, 4598–4601 (1995).
8. B. G. Klappauf, W. H. Oskay, D. A. Steck, and M. G. Raizen, "Observation of noise and dissipation effects on dynamical localization," Phys. Rev. Lett. **81**, 1203–1206 (1998); H. Ammann, R. Gray, I. Shvarchuck, and N. Christensen, "Quantum delta-kicked rotor: experimental observation of decoherence," Phys. Rev. Lett. **80**, 4111–4115 (1998).
9. L. Liu, "Talbot and Lau effects on incident beams of arbitrary wavefront, and their use," Appl. Opt. **28**, 4668–4678 (1989).
10. E. Ott, *Chaos in Dynamical Systems* (Cambridge U. Cambridge, UK, 1993).
11. P. Bergé, Y. Pomeau, and C. Vidal, *Order Within Chaos* (Hermann, Paris, 1984).
12. J. Guckenheimer and P. Holmes, *Nonlinear Oscillations, Dynamical Systems, and Bifurcations of Vector Fields* (Springer-Verlag, New York, 1983).
13. A. J. Lichtenberg and M. A. Lieberman, *Regular and Stochastic Motion* (Springer, New York, 1983).
14. M. C. Gutzwiller, *Chaos in Classical and Quantum Mechanics* (Springer, New York, 1990).
15. M. J. Giannoni, A. Voros, and J. Zinn-Justin, eds., "Chaos and quantum physics," in *Proceedings of the Les-Houches Summer School, Session LII, 1989* (North-Holland, Amsterdam, 1991).
16. G. L. Oppo, S. M. Barnett, E. Riis, and M. Wilkinson, eds., "Quantum dynamics of simple systems," in *Proceedings of the 44th Scottish Universities Summer School in Physics* (Scottish Universities Summer School in Physics Publications and Institute of Physics, Bristol, UK, 1996).
17. G. Casati, B. V. Chirikov, F. M. Izrailev, and J. Ford, in *Stochastic Behavior in Classical and Quantum Hamiltonian Systems*, Vol. 93 of Lecture Notes in Physics, G. Casati and J. Ford, eds. (Springer-Verlag, Berlin, 1979), p. 334.
18. B. V. Chirikov, F. M. Izrailev, and D. L. Shepelyansky, "Dynamical stochasticity in classical and quantum mechanics," Sov. Sci. Rev. Sect. C **2**, 209–267 (1981).
19. D. L. Shepelyansky, "Localization of quasienergy eigenfunctions in action space," Phys. Rev. Lett. **56**, 677–680 (1986); "Localization of diffusive excitation in multi-level systems," Physica D **28**, 103–114 (1987).
20. R. Blumel, S. Fishman, and U. Smilansky, "Excitation of molecular rotation by periodic microwave pulses. A testing ground for Anderson localization," J. Chem. Phys. **84**, 2604–2614 (1986).
21. R. Graham, M. Schlautmann, and P. Zoller, "Dynamical localization of atomic-beam deflection by a modulated standing light wave," Phys. Rev. A **45**, R19–R22 (1992); see also R. Graham, M. Schlautmann, and D. L. Shepelyansky, "Dynamical localization in Josephson junctions," Phys. Rev. Lett. **67**, 255–258 (1991), and references therein.
22. G. Casati, I. Guarneri, and D. L. Shepelyansky, "Hydrogen atom in monochromatic field: chaos and dynamical photonic localization," IEEE J. Quantum Electron. **24**, 1420–1444 (1988), and references therein; R. Blümel and U. Smilansky, "Microwave ionization of highly excited hydrogen atoms," Z. Phys. D **6**, 83–105 (1987), and references therein; E. J. Galvez, B. E. Sauer, L. Moorman, P. M. Koch, and D. Richards, "Microwave ionization of H atoms: breakdown of classical dynamics for high frequencies," Phys. Rev. Lett. **61**, 2011–2014 (1988); J. E. Bayfield, G. Casati, I. Guarneri, and D. W. Sokol, "Localization of classically chaotic diffusion for hydrogen atoms in microwave fields," Phys. Rev. Lett. **63**, 364–367 (1989), and references therein; R. Blümel, R. Graham, L. Sirko, U. Smilansky, H. Walther, and K. Yamada, "Microwave excitation of Rydberg atoms in the presence of noise," Phys. Rev. Lett. **62**, 341–344 (1989); R. Blümel, A. Buchleitner, R. Graham, L. Sirko, U. Smilansky, and H. Walther, "Dynamical localization in the microwave interaction of Rydberg atoms: the influence of noise," Phys. Rev. A **44**, 4521–4540 (1991), and references therein.
23. S. L. McCall, P. M. Platzman, R. Dalichaouch, D. Smith, and S. Schultz, "Microwave propagation in two-dimensional dielectric lattices," Phys. Rev. Lett. **67**, 2017–2020 (1991).
24. M. V. Berry and S. Klein, "Transparent mirrors: rays, waves, and localization," Eur. J. Phys. **18**, 222–228 (1997).
25. D. S. Wiersma, P. Bartolini, A. Lagendijk, and R. Righini, "Localization of light in a disordered medium," Nature **390**, 671–673 (1997).
26. J. Krug, "Optical analog of a kicked quantum oscillator," Phys. Rev. Lett. **59**, 2133–2136 (1987).
27. R. E. Prange and S. Fishman, "Experimental realizations of kicked quantum chaotic systems," Phys. Rev. Lett. **63**, 704–707 (1989); O. Agam, S. Fishman, and R. E. Prange, "Experimental realizations of quantum chaos in dielectric waveguides," Phys. Rev. A **45**, 6773–6802 (1992).
28. B. Fischer, A. Rosen, and S. Fishman, "Localization in frequency for periodically kicked light propagation in a dispersive single-mode fiber," Opt. Lett. **24**, 1463–1465 (1999).

29. B. Fischer, A. Rosen, A. Bekker, and S. Fishman, "Experimental observation of localization in the spatial frequency domain of a kicked optical system," Phys. Rev. E **61**, 4694R–4697R (2000).
30. D. R. Grempel, S. Fishman, and R. E. Prange, "Localization in an incommensurate potential: an exactly solvable model," Phys. Rev. Lett. **49**, 833–836 (1982).
31. See, for example, A. E. Siegman, *Lasers* (University Science, Mill Valley, Calif., 1986), Chap. 7.
32. I. Dana, E. Eisenberg, and N. Shnerb, "Dynamical localization near quantum antiresonance: exact results and a solvable case," Phys. Rev. Lett. **74**, 686–689 (1995); "Antiresonance and localization in quantum dynamics," Phys. Rev. E **54**, 5948–5963 (1996); E. Eisenberg and I. Dana, "Limited sensitivity to analyticity: a manifestation of quantum chaos," Found. Phys. **27**, 153–170 (1997).
33. R. E. Prange, D. R. Grempel, and S. Fishman, "Wave functions at a mobility edge: an example of a singular continuous spectrum," Phys. Rev. B **28**, 7370–7372 (1983); R. E. Prange, D. R. Grempel, and S. Fishman, "Solvable model of quantum motion in an incommensurate potential," Phys. Rev. B **29**, 6500–6512 (1984); R. E. Prange, D. R. Grempel, and S. Fishman, "Long-range resonance in Anderson insulators: finite-frequency conductivity of random and incommensurate systems," Phys. Rev. Lett. **53**, 1582–1585 (1984).
34. L. A. Pastur and A. L. Figotin, "Localization in an incommensurate potential: exactly solvable multidimensional model," JETP Lett. **37**, 686–688 (1983).
35. M. Ya. Azbel, "Energy spectrum of a conduction electron in a magnetic field," Sov. Phys. JETP **19**, 634–645 (1964).
36. S. Aubry and G. Andre, "Analyticity breaking and Anderson localization in incommensurate lattices," Ann. Isr. Phys. Soc. **3**, 133–164 (1979).
37. D. J. Thouless and Q. Niu, "Wavefunction scaling in a quasi-periodic potential," J. Phys. A **16**, 1911–1919 (1983).
38. M. Wilkinson, "Critical properties of electron eigenstates in incommensurate systems," Proc. R. Soc. London, Ser. A **391**, 305–350 (1984).
39. B. Simon, "Almost periodic Schrödinger operators: a review," Adv. Appl. Math. **3**, 463–490 (1982).
40. P. Sarnak, "Spectral behavior of quasi periodic potentials," Commun. Math. Phys. **84**, 377–401 (1982).
41. J. Avron and B. Simon, "Singular continuous spectrum for a class of almost periodic Jacobi matrices," Bull. Am. Math. Soc. **6**, 81–85 (1982); "Almost periodic Schrödinger operators. II. The integrated density of states," Duke Math. J. **50**, 369–391 (1983).